Available online at www.sciencedirect.com
SCIENCE DIRECT®
ELSEVIER
Journal of Crystal Growth 290 (2006) 319–333
JOURNAL OF CRYSTAL GROWTH
www.elsevier.com/locate/jcrysgro

Influence of oxygen, hydrogen, helium, argon and vacuum on the surface behavior of molten InSb, other semiconductors, and metals on silica

Arun K. Kota, Gaurav Anand, Suresh Ramakrishnan, Liya L. Regel*, William R. Wilcox

International Center for Gravity Materials Science and Applications, Clarkson University, Box 5705, Potsdam, NY 13699-5705, USA

Received 17 November 2005; accepted 10 January 2006
Available online 14 March 2006
Communicated by K.W. Benz

Abstract

Sessile drop experiments were performed on molten indium antimonide on clean quartz (fused silica) surfaces. A cell was constructed through which argon, helium, oxygen, hydrogen or a mixture of these was flowed at 600 °C. Some of the InSb was doped with 0.1% Ga. The surface tension σ of oxide-free molten InSb was smaller in Ar than in He, may have increased with increasing O_2 in the gas, and was not influenced by Ga or H_2. The contact angle θ on silica was higher in the presence of Ar, was lowered by O_2, and was not influenced by H_2 or Ga. The work of adhesion W and the surface energy σ_{sv} of the silica were higher in He than in Ar. The surface remained free of solid oxide only in flowing gas containing $\leqslant$0.8 ppm O_2. This behavior is attributed to reaction of O_2 at the surface of the melt to form In_2O gas. When solid oxide formed on Ga-doped material, it was strongly enriched in Ga, with the Ga/In ratio increasing with the concentration of O_2 in the gas.

Examination of published sessile-drop results for liquid metals and semiconductors on silica revealed that W and σ_{sv} were highest for reactive melts, in which SiO_2 dissolves. For non-reactive melts, W and σ_{sv} were lower and θ higher in a gas than in a vacuum, regardless of whether the experiments had been carried out in sealed ampoules, a flowing gas, or dynamic vacuum. The implication is that the surface of silica was different in a vacuum than in a gas at ~1 bar.
© 2006 Elsevier B.V. All rights reserved.

PACS: 68.10.Cr; 81.05.Ea; 81.10.Eq; 81.65.Mq

Keywords: A1. Contact angle; A1. Surface tension; A2. Growth from melt; B1. Metals; B2. Semiconducting materials

1. Introduction

In Bridgman crystal growth of semiconductors, fused silica[1] ampoules are typically used that have been evacuated and sealed, often after backfilling with helium or argon. However, at elevated temperature empty silica ampoules sealed in a high vacuum outgas to produce on the order of 10^{-4} bar of gas, which is predominantly hydrogen [1]. The interior of semiconductor growth ampoules is often coated with carbon to avoid sticking problems. Graphite converts the traces of water vapor outgassed from silica ampoules to H_2 and CO [1]. Crystal growth materials themselves contribute similar pressures of gases under such conditions, typically oxides and hydrogen [2]. Gases, particularly H_2, also diffuse through the ampoule wall [3]. Several percent of H_2 is frequently added to avoid formation of oxide that can cause sticking of the crystal to the ampoule wall, as well as formation of grains, twins and precipitates. Addition of H_2 to avoid oxide was essential in achieving detached solidification[2] (e.g., Ref. [4])

*Corresponding author. Fax: +1 315 268 6654.
E-mail address: regel@clarkson.edu (L.L. Regel).

[1]Amorphous fused silica is frequently called "quartz," albeit incorrectly as true quartz is crystalline.

[2]In detached solidification, also called "dewetting," the solid grows without contact with the ampoule wall, i.e., there is a separation between some portion of the ingot and the wall.

0022-0248/$ - see front matter © 2006 Elsevier B.V. All rights reserved.
doi:10.1016/j.jcrysgro.2006.01.044

of Ga-doped InSb on Earth [5]. HgZnTe grew detached if a carbon getter was included in the ampoule [6,7].

Impurities have been implicated in detached solidification by increasing the melt-ampoule contact angle θ, which theory indicates should favor detachment (e.g., Refs. [8,9]). Duffar et al. [10] wrote that "*semiconductors can present very high contact angles on crucible materials, due to slight amounts of pollution by residual gases. This phenomena is used to explain the de-wetting of semiconductors observed when grown under microgravity conditions in smooth crucibles.*" The basis for this conclusion was their observation made in sessile-drop experiments with InSb on silica [10]. As described in Ref. [9], "*it was practically always necessary to shake the molten drops a little bit in order to measure the contact angle corresponding to thermodynamic equilibrium* (112° *in this particular case*), *otherwise contact angles as high as* 170° *might have been measured. This effect is attributed to absorption of some impurity at the surface of the drop which creates a layer subsequently removed when shaking. In any case this layer cannot be confused with a solid peel on the drops which were always perfectly clean and shiny before, during and after the experiments. The vacuum in the ampoules during sealing was below* 10^{-7} mbar." This was the motivation for the study reported here.

The most likely impurity that interacts strongly with molten semiconductors was believed to be oxygen. This is because numerous experiments with liquid metals on oxide surfaces had shown that oxygen always lowers the surface tension σ of metals and dramatically lowers the contact angle θ when it exceeds a critical value ranging from $\sim 10^{-19}$ bar for Sn to $\sim 10^{-5}$ bar for Ag (e.g., Refs. [11–16]). The evidence is that O_2 dissociates when it dissolves in liquid metals, adsorbs on the melt–vapor surface, and modifies the melt–oxide substrate surface. Silicon is the only semiconductor for which the influence of O_2 on surface properties has been extensively investigated. Sessile-drop experiments showed that O_2 lowers the surface tension of molten silicon [17–22]. Huang et al. [17] displayed their data versus the partial pressure of oxygen, while Niu et al. [18–20] correlated their results versus the square root of the oxygen pressure based on oxygen dissociating upon entering molten Si. Huang et al. [17] also found that the contact angle of the melt on pyrolytic boron nitride (pBN) "decreased a little" with increasing oxygen partial pressure up to $\sim 4 \times 10^{-4}$ bar. They measured higher oxygen and boron concentrations on the surface of frozen drops than in their interior. Kaiser et al. [23] determined that the surface tension of Ge on pBN was lower in Ar or high vacuum than in Ar containing 2% H_2, while values were lower on glassy carbon substrates in a vacuum. This indicates that H_2 increases σ of Ge and O_2 decreases σ of Ge.

2. Experimental apparatus and methods

Details of the experimental apparatus and methods are given elsewhere [24–26]. A schematic diagram of the apparatus is shown in Fig. 1. It consisted of the following parts:

- A Thermcraft three-zone split tube furnace to melt the InSb and maintain the resulting drop at the desired temperature.
- A cell containing a fused silica substrate to support the sessile drop (Fig. 2).
- A system to flow a gas of desired composition through the cell. This system contained
  - an oxygen analyzer to measure the fugacity (partial pressure for an ideal gas) of oxygen in the gas flowing out of the cell,

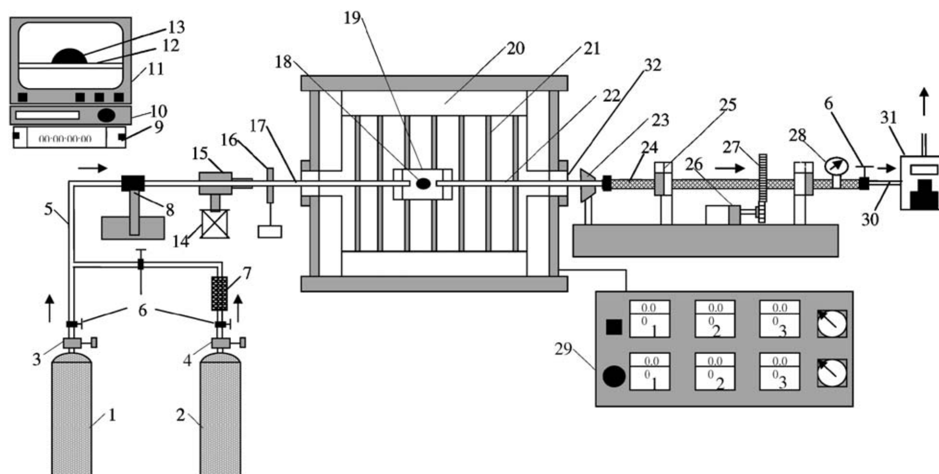

Fig. 1. Sessile drop apparatus. (1) Ar with desired O_2 content, (2) mixture of 90%Ar and 10% H_2, (3) CGA 580 pressure regulator, (4) CGA 350 pressure regulator, (5) $\frac{1}{4}''$ copper tube, (6) ball valve, (7) Oxisorb, (8) inlet support, (9) time code generator, (10) VCR, (11) monitor, (12) substrate in the display, (13) InSb drop in the display, (14) optical bench, (15) camera with the lens, (16) filter, (17) inlet tube of cell, (18) InSb sessile drop, (19) chamber with fused silica substrate, (20) furnace insulation, (21) SiC heating elements, (22) outlet tube of cell, (23) light source, (24) $\frac{1}{2}''$ stainless steel pipe, (25) bearings, (26) motor, (27) gear, (28) pressure gauge, (29) temperature controller, (30) $\frac{1}{8}''$ stainless steel tube, (31) oxygen analyzer, (32) optical quality fused silica disc.

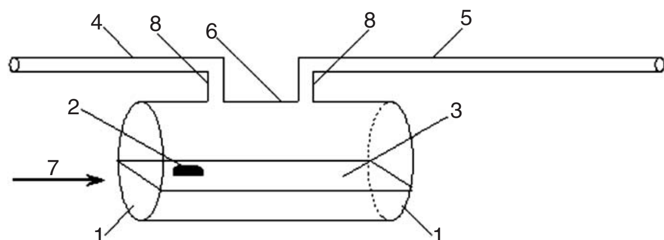

Fig. 2. Schematic diagram of the cell. (1) Ground and polished optical quality fused silica discs (26–30 mm ID), (2) InSb sessile drop, (3) fused silica microscope slide, (4) fused silica inlet gas tube (8-mm ID), (5) fused silica outlet gas tube (8 mm ID), (6) fused silica cylinder (26–30 mm ID and 45–75 mm long), (7) view of the CCD video camera, (8) riser for inlet and outlet gas tubes (15 mm).

  - ○ supporting structures to hold the cell suspended in the furnace and a motor–gear assembly to tilt the cell.
- An optical system to record the drop profile at intervals during an experiment.

Several gases were used in the experiments, including industrial-grade Ar, ultra-high purity (UHP) Ar, UHP Ar premixed with 10% H_2, scientific-grade He, Ar with 3 ppm O_2 added, and Ar with 6 ppm O_2. Argon is extracted from air by distillation. Since the vapor pressures of O_2 and Ar do not differ widely, it is virtually impossible to remove all O_2 from Ar. For that reason, later experiments were performed in He. Our gas supplier (Merriam-Graves: MG Industries) specified their industrial grade Ar as containing <8 ppm O_2 and <5 ppm moisture, UHP Ar with <1 ppm O_2 and <1 ppm moisture, and scientific He <0.5 ppm of both O_2 and H_2O. An Oxisorb® oxygen removal unit[3] was used to reduce O_2 and moisture in some experiments, and appeared to influence the results only in its effect on oxygen concentration.

The O_2 concentration in the gas flowing out of the experiment cell was measured by a DF-150 non-depleting coulometric oxygen analyzer.[4] It is able to measure O_2 concentrations between 0.01 and 10 ppm at pressures in the range ± 5 psig. It was used here at a total pressure from 1.1 to 1.5 bar and flow rate from 1 to 3 cubic feet per minute (1.7–5.1 m^3/h). After purging the apparatus for 1 day with industrial Ar this analyzer showed 0.6–0.7 ppm O_2, 0.3 ppm O_2 after purging with UHP Ar for 1 day, and 0.08 ppm O_2 with He for 3 days. In successful experiments yielding shiny mobile drops, the O_2 partial pressure was $\leqslant 9 \times 10^{-7}$ bar.

The silica cell was soaked in aqua regia for 1 day to remove organic and metallic contaminants, and rinsed with deionized water, acetone and methanol. For 11 experiments on undoped InSb the resulting cell was held at 1100 °C for 1 day while purging with a 10% H_2–Ar mixture in order to eliminate adsorbed water. Five experiments on Ga-doped InSb were performed using cells that had been purged at 750 °C for 10 h. The results of a sixth experiment on Ga-doped InSb with 1100 °C preheating were indistinguishable from those purged at 750 °C. Each cell was used for 3–6 experiments, with no systematic change in results noted from one experiment to the next. Examination of the silica substrate after experiments and removal of the frozen drop did not reveal any change in the substrate surface.

InSb pieces weighing 0.3–0.5 g were broken from zone-refined material.[5] Each sample was soaked in dilute HCl for half a day, rinsed with methanol in an ultrasonic bath, dried, and placed in the cell. If the cell had been preheated at 1100 °C, the sample was introduced before the cell had completely cooled, while avoiding the introduction of air as much as possible. The cell with sample was rapidly heated to 400 °C and held for 1 day in flowing 10% H_2–Ar. The desired gas was passed through the cell for half a day at 400 °C. The temperature was increased to 600 °C and held until the oxygen concentration no longer changed, approximately 2 days, before recording images for analysis. All of the results reported here were obtained at 600 °C, with no detectable difference from results obtained on Ga-doped material at 550 and 650 °C.

Preliminary experiments revealed that excess vibration caused the surface of the sessile drop to shake, making measurement inaccurate. Additionally, in attempting to measure contact-angle hysteresis by tilting the substrate, this vibration led to premature rolling of the drop down the incline. In order to eliminate the effects of the vibration, the end supports for the cell were placed on vibration damping pads with metal weights to depress the pads.

A black and white CCD camera[6] fitted with a 10 × zoom lens was used to view the drop through the gas-entry end of the furnace. A 100-W bare light bulb was placed at the other end of the furnace, so that the drop was seen as a silhouette. A welding filter was placed between the CCD camera and the furnace to eliminate haziness in the video picture. The camera assembly was mounted on an optical bench that could be moved in both directions perpendicular to the axis of view. The view of the drop was displayed on a monitor and recorded using either a computer with an image card or a videocassette recorder[7] with later transfer to the computer with a frame grabber.

When a solid sample first melted, oxide could be seen on the surface of the resulting drop that prevented it from moving. Exposure to 10% H_2–Ar expedited achievement of a shiny drop that moved freely when the cell was tilted or tapped (much like a drop of clean mercury on glass), although lengthy heating in UHP Ar produced the same result. This change is attributed to the gradual elimination of oxide. A shiny Ga-doped InSb drop could not be maintained in the absence of H_2 if the gas contained more

[3]From Air Liquide Deutschland GmbH, Krefeld, Germany, http://www.spezialgase.de.

[4]From Delta F Corporation, Woburn, Massachusetts, http://www.delta-f.com.

[5]Kindly provided by Firebird Semiconductors in Trail, British Columbia, Canada.

[6]Sony SSC-M374.

[7]Sanyo 4 Head/Field Advance.

Fig. 3. Image of a drop grabbed from a videotape of an experiment on Ga-doped InSb in Ar and 2.0×10^{-7} bar O_2. Note that there is no reflection of the drop on the substrate surface, indicating that the camera is properly aligned with the substrate.

Fig. 4. Image of a drop on a tilted substrate from an experiment on Ga-doped InSb in Ar and 2.8×10^{-7} bar O_2. This image was grabbed just before the drop rolled down the substrate.

than 0.8 ppm O_2. Fig. 3 shows an image of a drop on a near-horizontal substrate and Fig. 4 shows a drop on a tilted substrate just prior to the drop rolling to the side. An experiment was deemed successful, and the results reported here, only if the drop remained shiny and readily moved when the cell was tapped or tilted.

Six successful sessile drop experiments were performed using Ga-doped InSb and 10 with undoped material. Three of each of these were done in the presence of 10%H_2-Ar, while Ar was always present when Ga-doped InSb was used. Seven experiments on undoped material were performed in He. The O_2 partial pressure was varied from 0.97 to 9.0×10^{-7} bar. Higher oxygen concentrations tended to make the surface of a drop dull and prevent it from moving, particularly for Ga-doped material. Prior to grabbing an image for analysis, the substrate was tilted so as to position the drop, the substrate was made as horizontal as possible, and the cell was tapped to avoid contact line sticking, sometimes vigorously enough to cause the drop to briefly "jump" from the substrate.

Two to five images from each experiment were analyzed, for a total of 57 digital images. Between each image the drop was moved by tapping and/or rotating the cell clockwise and counterclockwise. While each image was slightly different, there was no trend with time. The images were analyzed using automated algorithms that required little or no manual input, in order to improve reproducibility and provide freedom from operator bias. First, a MATLAB program produced a binary image of the edge of the drop. This program finds edges using the Prewitt approximation [27] to the derivative, and returns edges at those points where the gradient of the image is a maximum. The region of interest was selected using Microsoft Windows' Paint. The substrate edge was removed using the "fill with color" tool to convert the substrate's pixels to black, so that only the drop outline remained. The pixel coordinates of the drop surface were determined using the measurement tool of HLImage++98 software.[8] Another MATLAB program converted the pixel positions into SI coordinates. The calibration was done using a frame from the CCD camera focused on a sheet of graph paper inside the furnace at the same location as the drop. Another MATLAB program determined the contact points and the maximum height of the drop directly from the drop coordinates. The drop coordinates, contact points and height were input to the ADSA-P[9] FORTRAN program [28,29], which determines the surface tension σ and the contact angle θ best fitting the drop edge coordinates to the theoretical shape in a gravitational field [30]. Values for θ were also determined using polynomial fits to the drop surface near the left and right contact points for one image from each experiment. The resulting left and right contact angles differed by an average of 1.9° from one another, but in a random way. The value of θ from ADSA-P was usually larger than that from the polynomial method, with the difference Δ tending to increase with θ according to the equation $\Delta = 0.4\theta - 53^\circ$ ($R^2 = 0.58$).[10] The polynomial results produced the same trends as those reported below but with less statistical certainty. Because the polynomial method provides no values for σ and because fewer images were analyzed, only the ADSA-P results are reported here.

Contact-line sticking can inhibit motion of a sessile drop, which probably accounts for the observation of Duffar et al. [8,9] quoted above. This causes the contact angle of a moving drop to deviate from the equilibrium static value, increasing the contact angle at the advancing contact line

[8] Western Vision Software, http://www.wvision.com/.

[9] Axisymmetric Drop Shape Analysis—Profile.

[10] R is the correlation coefficient, and R^2 is the fraction of the variation in dependent variable (here, Δ) that is explained by the correlating equation.

and decreasing the contact angle at the retreating contact line. The difference between advancing and retreating contact angles is known as contact-angle hysteresis. In has been found, for example, that the hysteresis of mercury drops on glass is greater in air with ~50% relative humidity than in dry nitrogen, presumably because of oxide formation [31]. An indication of contact-angle hysteresis can be obtained by tilting the substrate on which the drop rests (e.g., Ref. [32]). Contact-line sticking causes the upper contact angle to decrease and the lower contact angle to increase. As the substrate is tilted farther, eventually the contact-line sticking is insufficient to prevent the drop from rolling down the surface.

Contact-angle hysteresis was measured for Ga-doped InSb drops. Hysteresis is defined here as the difference between the contact angles on the two sides of the drop on the video frame just prior to that in which the drop rolled down the substrate as it was slowly tilted. The left and right contact angles were estimated by aligning tangents on the two sides of the drop using HLImage + + 98.

3. Experimental results

Addition of 10% H_2 to the UHP Ar gas did produce a measurable decrease in the oxygen concentration of the gas entering the oxygen analyzer. Sudden changes in furnace temperature also shifted the oxygen analyzer results. For example, when the furnace temperature was increased by 50 °C with Ga-doped InSb, there was an almost instantaneous decrease of 0.02–0.05 ppm in the oxygen analyzer reading, which subsequently increased and stabilized at the value existing before the change in temperature. This all transpired in 1–2 min. When the temperature was decreased to the original value, the reverse process occurred.

The frozen drops from the experiments were examined by optical microscopy, scanning electron microscopy (SEM) and energy dispersive X-ray spectroscopy (EDX) in the SEM. Each frozen drop was rounded with one or more protrusions, as shown in Fig. 5. Such protrusions are well known when group IV, III–V and II–VI semiconductors are frozen, and arise because the melt has a greater density than the corresponding solid. Sessile drops that were shiny and moved easily on the substrate always had a dull surface when they were frozen, while the protrusions remained shiny. SEM of the dull regions revealed dark islands, as shown in Fig. 6. These islands were smaller when gas containing 10% hydrogen was used, and were both smaller and less distinct on undoped InSb. EDX spectra of these dull regions had O peaks, and strong Ga peaks on Ga-doped material. The protrusions showed no Ga or O EDX peaks.

Molten drops of Ga-doped InSb that were not shiny or mobile formed frozen drops with rough thick black coatings. (No such drops were used to generate the contact angle and surface tension values given here.) Fig. 7 shows a cross section of such a coating. As seen in Fig. 8, EDX spectra of these coatings displayed peaks not only for In, Sb and O, but also a strong peak for Ga. EDX of the Ga-doped starting material showed no Ga peak. Glow-discharge mass-spectroscopy of a piece of the Ga-doped starting material was performed by the Institute for

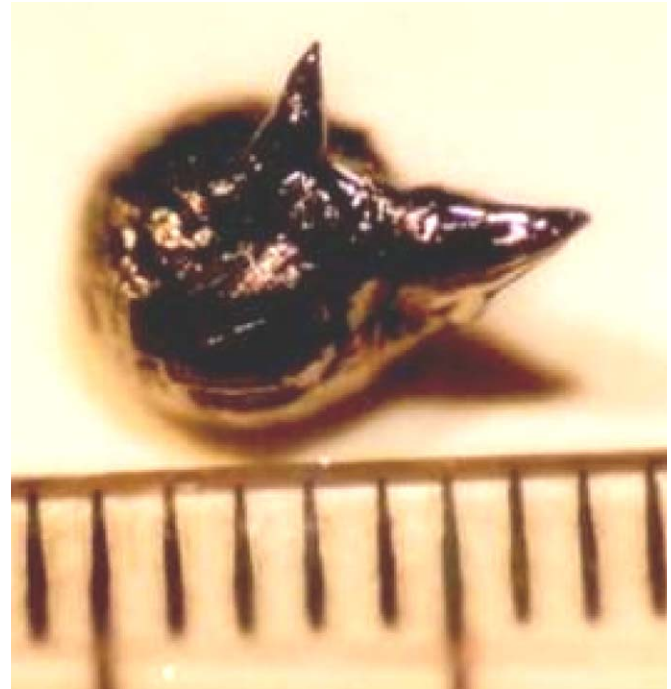

Fig. 5. Image of a frozen drop resulting from an experiment on Ga-doped InSb in Ar with 10% H_2 and 2.0×10^{-7} bar O_2. Notice that the edges of the sample are rounded and there are two shiny protrusions. The scale is in mm.

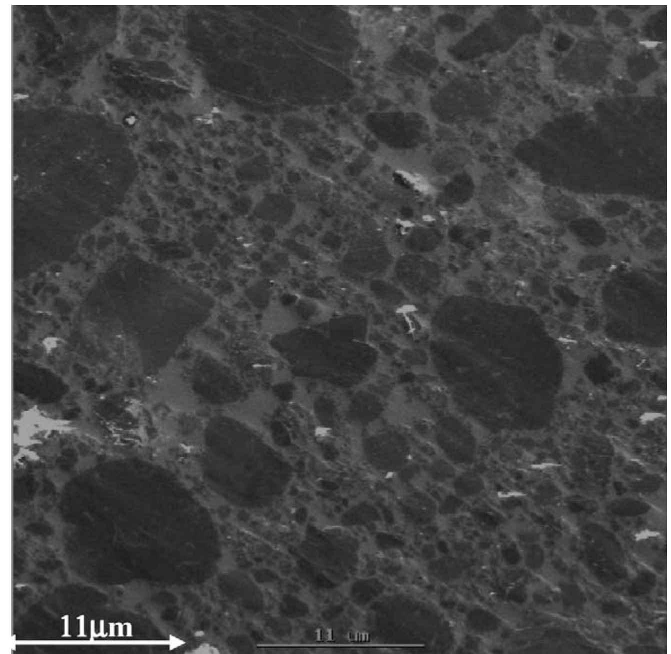

Fig. 6. Scanning electron micrograph of a dull portion of the frozen drop from an experiment on Ga-doped InSb performed in Ar with 10% H_2 and 2.3×10^{-7} bar O_2. The black islands are oxide.

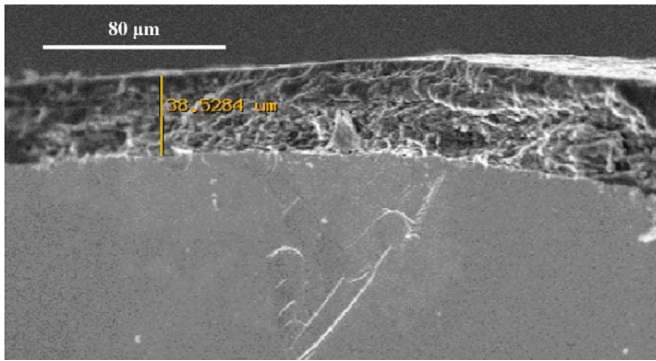

Fig. 7. Cross section of a heavily oxidized frozen drop of Ga-doped InSb. The oxide layer is about 40 μm thick.

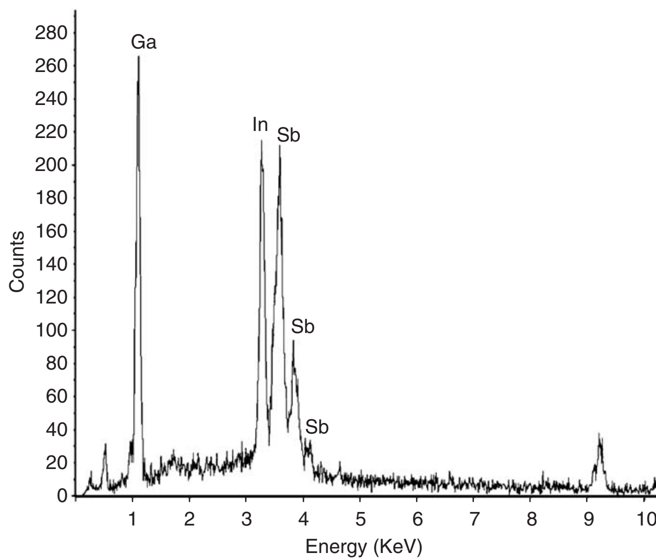

Fig. 8. EDX spectra of the surface of an oxidized frozen drop of Ga-doped InSb. Note the peaks for oxygen, gallium, indium and antimony.

National Measurement Standard, National Research Council, Canada, and showed approximately 0.1 at% Ga. This Ga concentration is below the detection limit of our EDX. As shown in Fig. 9, the ratio of Ga to In peak heights of the surface of oxidized drops increased with increasing oxygen concentration during the experiment. (No measurements were made on frozen clean, i.e. shiny, drops.) That is, the Ga-enrichment of the oxide on the surface of frozen drops increased with increasing oxygen concentration in the gas. The data shown in Fig. 8 were correlated by two different equations:

$$\mathrm{Ga/In} = 0.26 + 1.4 \times 10^5\, P_{O_2}$$
$$(R^2 = 0.84,\ p = 0.041,\ F\text{-significance} = 0.083), \qquad (1)$$

$$\mathrm{Ga/In} = 420\sqrt{P_{O_2}}$$
$$(R^2 = 0.87,\ p = 0.001,\ F\text{-significance} = 0.047), \qquad (2)$$

where Ga/In is the ratio of EDX peak heights, P_{O_2} is the oxygen partial pressure in bar, p is the probability that the true slope differs in sign from that found, and "*F*-significance" is the probability that there is no dependence of Ga/In on P_{O_2} or $\sqrt{P_{O_2}}$. Thus, the best correlation is that giving the highest R^2, lowest p, lowest *F*-significance, and a 0 intercept, i.e. Eq. (1).

Correlations of the ADSA-P results are given in Table 1, where θ is the contact angle in degrees, σ is the gas–liquid surface tension in $\mathrm{N/m} = \mathrm{J/m^2}$, X_{Ga} is the atom fraction of Ga in the melt (0 or 0.001), Y_{H_2} is the mole fraction of H_2 in the gas (0 or 0.1), P_{O_2} is the measured partial pressure of O_2 in the gas in bar, and $Y_{Ar} = 1$ if Ar or Ar + H_2 was used and 0 if He was used. Excel's Regression tool was used to fit the following equations:

$$\sigma = A_0 + A_{O_2}P_{O_2} + A_{Ga}X_{Ga} + A_{H_2}Y_{H_2} + A_{Ar}Y_{Ar}, \qquad (3)$$

$$\theta = B_0 + B_{O_2}P_{O_2} + B_{Ga}X_{Ga} + B_{H_2}Y_{H_2} + B_{Ar}Y_{Ar}, \qquad (4)$$

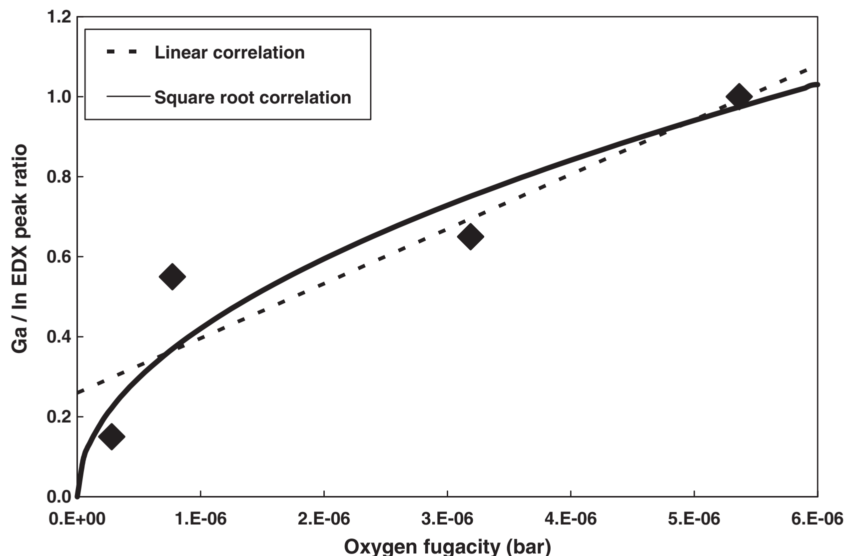

Fig. 9. The influence of oxygen fugacity (partial pressure) on the ratio of the peak heights of Ga and In in the EDX spectra on frozen oxidized drops.

Table 1
Correlations of the ADSA-P results using Eqs. (3) and (4)

Experimental conditions	Gas	Argon				Helium	All data		
	X_{Ga}	0	0.001	0.001	All data with	0	All included	Y_{Ar} not included	Only Y_{Ar} always inc
	Y_{H_2}	0.1	0	0.1	argon	0			
Correlations for gas–melt surface tension, σ	Mean	0.40±0.03	0.39±0.02	0.38±0.01	0.39±0.02	0.48±0.02	0.42±0.02		
	R^2	0	0	0.54	0.12	0.01	0.69	0.43	**0.67**
	F-sig	1	1	0.016	0.31	0.64	7.5×10^{-7}	1.3×10^{-6}	$\mathbf{1.5\times10^{-8}}$
	A_0	0.40±0.04	0.39±0.02	0.37±0.01	0.41±0.05	0.47±0.03	0.47±0.02	0.46±0.02	**0.47±0.02**
	A_{O_2} ()	0	0	$2\pm1\times10^4$ (0.008)	$6\pm8\times10^4$ (0.07)	$2\pm10\times10^4$ (0.32)	$4\pm6\times10^4$ (0.09)	$6\pm6\times10^4$ (0.05)	**N/I**
	A_{Ga} (p)	N/A	N/A	N/A	−40±40 (0.04)	N/A	−30±40 (0.08)	−60±30 (9×10^{-5})	**N/I**
	A_{H_2} ()	N/A	N/A	N/A	−0.2±0.4 (0.13)	N/A	−0.2±0.5 (0.19)	−0.6±0.3 (8×10^{-5})	**N/I**
	A_{Ar} (p)	N/A	N/A	N/A	N/A	N/A	−0.06±0.06 (0.023)	N/I	**−0.09±0.03 (8×10^{-9})**
Correlations for contact angle, θ	Mean	158±3	159±1	158±2	158±2	143±1	152±2		
	R^2	0	0	0.63	0.07	0.37	0.92	0.69	**0.91**
	F-sig	1	1	0.006	0.54	0.002	4.1×10^{-20}	1.6×10^{-13}	$\mathbf{5.4\times10^{-22}}$
	B_0	158±3	159±1	162±3	159±5	144±1	144±2	147±2	**144±2**
	B_{O_2} ()	0	0	$-8\pm5\times10^6$ (0.003)	$-6\pm9\times10^6$ (0.08)	$-8\pm5\times10^6$ (0.001)	$-7\pm5\times10^6$ (0.002)	$-10\pm7\times10^6$ (0.001)	$\mathbf{-6\pm4\times10^6}$ **(0.002)**
	B_{Ga} (p)	N/A	N/A	N/A	$0.2\pm0.4\times10^4$ (0.23)	N/A	$2\pm3\times10^3$ (0.13)	$1.0\pm0.3\times10^4$ (6×10^{-9})	**N/I**
	B_{H_2} ()	N/A	N/A	N/A	8±44 (0.35)	N/A	10±30 (0.28)	110±30 (9×10^{-11})	**N/I**
	B_{Ar} (p)	N/A	N/A	N/A	N/A	N/A	15±4 (2.4×10^{-9})	N/I	**16±2 (6.7×10^{-23})**

The ± represent 95% confidence limits. The p is the probability that the sign of the coefficient differs from that shown.
The best correlations in the table are those in the last column, which is in bold.
N/A means not applicable, i.e. this parameter was not varied. N/I means this variable was not included in the correlating equation.

where the A's and B's are coefficients giving the largest R^2. The $\pm$ values in Table 1 are 95% confidence limits. That is, there is a 5% chance the true value is outside the given range. To help interpret the statistical parameters shown in Table 1, let us look at the influence of P_{O_2} on θ for the subset of the data for $X_{Ga} = 0.001$ and $Y_{H_2} = 0.1$. We see that the equation $\theta = B_0 + B_{O_2} P_{O_2}$ with $B_0 = 162^\circ$ and $B_{O_2} = -8 \times 10^6$ deg/bar explains 63% (R^2) of the variation in θ. There is 95% probability that the true value of B_0 lies between 159° and 165°, and that the true value of B_{O_2} lies between -3×10^6 and -13×10^6 deg/bar. There is 0.3% chance (p) that the true value of B_{O_2} is actually positive, and a 0.6% chance (F-sig) that θ does not depend on P_{O_2} at all.

The last three columns include all of the data. The correlations in the column on the left include all parameters, the middle column correlations exclude Y_{Ar} as a variable, and the correlations on the right always include Y_{Ar}. The best correlations, i.e. those with the smallest F-sig, are those in the last column on the right.

For contact angle θ, an even better fit to all of the data was obtained by the following equation:

$$\cos(\theta) = -0.80 \pm 0.01 + 6 \pm 3 \times 10^4\, P_{O_2} - 0.14 \pm 0.01\, Y_{Ar}$$
$$(p = 0.0005) \qquad (p = 1 \times 10^{-26})$$
$$(R^2 = 0.94,\ F - \text{significance} = 2 \times 10^{-25}). \tag{5}$$

The angle of tilt at which a Ga-doped drop in Ar rolled down the silica substrate ranged from 0.005° to 8.2°, and averaged 1.6°. (Drops that remained oxidized would not move at any angle.) The hysteresis ranged from 1° to 14°, and averaged 7°. There was no correlation of these parameters with one another or with temperature, P_{O_2}, or Y_{H_2}. An interesting observation was made on the motion of shiny Ga-doped InSb drops when the cell was tilted. Sometimes the drop would begin to move at a low tilt angle and then stop, and not move again until the angle was increased. In experiments with the undoped material, it was determined that the spot where such sticking occurred corresponded to the drop's initial location (where it formed by melting the solid feed and remained while removing oxide during the purge cycle).

technique [33]. For σ was found a value of 0.43 N/m, which is near those found in the present work. On the other hand, θ was reported as 112°, which is significantly lower than the values obtained here, both by ADSA-P and by the polynomial method. The intriguing results of Kaiser et al. [23] for Ge on silica are highly relevant. They discovered that θ was significantly higher (~155°) in flowing Ar than in a dynamic vacuum (~115°), with the shift between the two being reversible. However, the change in θ was much slower, requiring ~60 h, when they shifted to a vacuum from Ar than vice versa. A layer on the surface of the drop was observed after some time in Ar that subsequently disappeared in the dynamic vacuum. These results hint at the complexity of the semiconductor/silica/gas system. We will now attempt to resolve these complexities.

The starting point in interpreting contact angle data is the classical Young equation, which relates the contact angle θ to three surface energies in the system (e.g., Refs. [11,34,35]):

$$\cos\theta = \frac{\sigma_{sv} - \sigma_{sl}}{\sigma}, \tag{6}$$

where σ_{sv} is the energy (J/m^2) of the solid–vapor surface and σ_{sl} is the solid–melt surface energy. For $\theta > 90^\circ$ as here, $\cos\theta < 0$, indicating that $\sigma_{sl} > \sigma_{sv}$. The value of $\sigma_{sv} - \sigma_{sl} = \sigma \cos\theta$ can be obtained from experimental values of σ and θ. Neumann et al. (e.g., Refs. [36,37]) pointed out that $\sigma\cos\theta$ is a function of σ alone if "at constant σ_{sv}, intermolecular forces (or surface tension components) do not have any independent effects on the contact angles"[36]. A plot of our data in Fig. 10 as $\sigma\cos\theta$ versus σ revealed that the data fall on two lines, one corresponding to measurements made in He and the other to experiments in Ar or Ar + 10% H_2. A measure of the relative variation in values is the standard deviation divided by the mean, which is 0.15 for σ and 0.08 for $\cos\theta$. Following Refs. [36,37], we conclude that σ_{sv} was constant on each line and so was higher in the presence of He than in Ar. This is a highly surprising result. Furthermore, the different slopes of the lines in Fig. 10 imply that whatever caused σ to increase also caused σ_{sl} to increase by about the same amount in Ar, but only by $\frac{3}{4}$ of this amount in He. Additionally, correlation of $\sigma\cos\theta$ yields

$$\sigma_{sv} - \sigma_{sl} = \sigma\cos\theta = 0.04 \pm 0.04 + 3 \pm 2 \times 10^4\, P_{O_2} - 0.06 \pm 0.01\, Y_{Ar} - 0.88 \pm 0.07\sigma$$
$$(p = 0.02) \quad (p = 0.002) \quad (p = 1 \times 10^{-18}) \quad (p = 1 \times 10^{-30}) \tag{7}$$

with $R^2 = 0.96$ and F-significance $= 7 \times 10^{-29}$.

How do these results compare with literature data for liquid metals and semiconductors on silica? Available data were compiled in Table 2 and are plotted in Fig. 11. These data appear to fall on three lines, which can be identified (with two exceptions) as belonging to the following classes:

4. Analysis and discussion

4.1. Surface tension and contact angle

The most recent measurements reported in the literature for σ and θ of molten InSb on SiO_2 were performed in a static vacuum (sealed ampoule) using the sessile drop

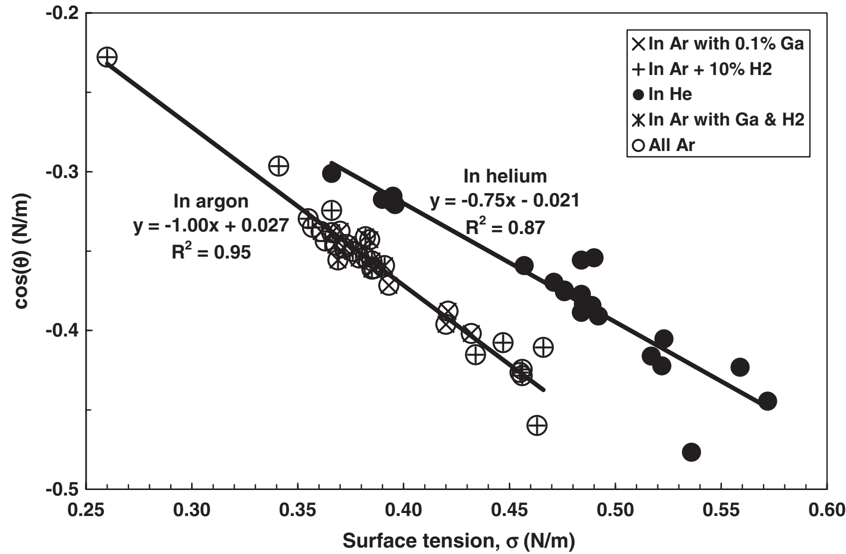

Fig. 10. Plot of experimental values of surface tension σ and contact angle θ for InSb, in Ar or He, undoped and doped with 0.1% Ga, and with and without 10% H_2 in the argon.

- Reactive melts, according to the classification of Refs. [11,15], i.e. melts in which the silica substrate dissolves to give an appreciable oxygen concentration.
- Non-reactive melts in a vacuum, either static or dynamic.
- Non-reactive melts in a gas at ~1 bar.

The two exceptions are Pb in He, the point for which (■) falls near the correlation for non-reactive melts in vacuum, and Au in a vacuum (●), which is near the correlation for non-reactive melts in a gas.

Also shown in Table 2 is the work of adhesion of the melt on the substrate:

$$W \equiv \sigma_{sv} + \sigma - \sigma_{sl} = \sigma(1 + \cos\theta), \tag{8}$$

which is known as the Young–Dupré equation (e.g., Ref. [11]). Note that W, on average, is highest for reactive melts and lowest for non-reactive melts in a gas.

The relative positions of the three sets of data in Fig. 11 imply that the solid–vapor surface energy, σ_{sv}, is highest for reactive melts and lowest for non-reactive melts in a gas. There are two methods that can be used to obtain estimates of σ_{sv} from measurements of σ and θ. By combining the equation suggested by Good [45] with Young's equation, we find one:

$$\sigma_{sv} \approx \frac{\sigma(1 + \cos\theta)^2}{4\Phi_{sl}^2}, \tag{9}$$

where Φ_{sl} "is a function of the molecular properties of the liquid and the solid, and rather than lies between about 0.5 and 1.0 for common systems in which contact angles are observed" [45]. Thus $\sigma(1+\cos\theta)^2/4$ is also given in Table 2, and would equal σ_{sv} if $\Phi_{sl} = 1$. A second method for estimate σ_{sv} is obtained by combining the result of the equation-of-state approach of Refs. [37,46] with Young's equation:

$$\cos\theta = -1 + 2\sqrt{\frac{\sigma_{sv}}{\sigma}}\, e^{-\beta(\sigma - \sigma_{sv})^2}, \tag{10}$$

where β was determined to be 124.7 N/m by fitting data [37,46]. Comparison of Eqs. (9) and (10) gives $\Phi_{sl} = e^{-\beta(\sigma-\sigma_{sv})^2}$. Table 2 also shows values of σ_{sv} found by solving Eq. (10) for experimental values of θ and σ. While Eq. (9) with $\Phi_{sl} = 1$ gives much lower values than Eq. (10), both yield the highest solid surface energies for reactive melts and the lowest for non-reactive melts in a vacuum. Experimental values for the surface energy of silica in the literature include 0.18 N/m at 1000 °C [47] and 0.33 N/m at 1727 °C [48,49]. A theoretical estimate for a fresh fracture surface at room temperature is 1.5 N/m [50].

In the following sections we try to separate the influences of the choice of gas and Ga-doping on the surface properties of InSb in particular, as well as for liquid metals and semiconductors in general.

4.2. Influence of reactivity of the melt

Table 2 shows that the so-called reactive melts have the highest σ, lowest average θ and highest work of adhesion W. They also tend to adhere strongly to silica when they freeze, sometimes leading to fracture of the silica. One expects these melts to continually remove the surface of the silica and any adsorbed species such as water (see Section 4.3). Thus, these melts interact with virgin silica. Interestingly, they also appear to produce the highest estimated σ_{sv} for silica, which implies that these melts change the silica surface adjacent to the drop as well as that between the drop and the silica.

Table 2
Average literature values for liquid metals and semiconductors on silica

Material	Atmosphere	Surface ten (σ) (N/m)	Contact ang (θ) (deg)	$\sigma \cos\theta$ ($\sigma_{sv}-\sigma_{sl}$) (N/m)	σ $(1+\cos\theta)$ (W) (N/m)	$\sigma(1+\cos\theta)^2/4$ σ_{sv} if $\Phi_{sl}=1$ (N/m)	σ_{sv} via Eq. (10) (N/m)	Source (Ref.)
Non-reactive melts in vacuum, either in sealed ampoules or connected to a vacuum system ("dynamic vacuum")								
Au	Vacuum	1.127	143	−0.900	0.227	0.011	0.994	[38]
CdTe	Vacuum	0.180	80	0.031	0.211	0.062	0.255	[39]
Cu	Vacuum	1.233	128	−0.759	0.474	0.046	1.120	Through [38]
$Fe_{78}B_{13}Si_9$	Vacuum	1.000	123	−0.545	0.455	0.052	0.893	[40]
Ga	Vacuum	0.646	119	−0.313	0.333	0.043	0.549	Through [38]
GaAs	Vacuum	0.450	120	−0.225	0.225	0.028	0.349	[41]
GaSb	Vacuum	0.453	121	−0.233	0.220	0.027	0.351	[11]
Ge	Vacuum	0.570	117	−0.259	0.311	0.042	0.472	[23]
Hg	Vacuum	0.482	100	−0.084	0.398	0.082	0.402	[42]
In	Vacuum	0.540	128	−0.332	0.208	0.020	0.429	Through [38]
InSb	Vacuum	0.434	112	−0.163	0.271	0.042	0.342	[11]
Sb	Vacuum	0.360	114	−0.146	0.214	0.032	0.268	Through [11]
Sn	Vacuum	0.510	112.5	−0.195	0.315	0.049	0.417	[43]
Sn	Vacuum	0.464	125	−0.266	0.198	0.021	0.357	Through [38]
	Averages:	0.604	117	−0.314	0.290	0.040	0.514	
Non-reactive melts in gas at ~1 bar, either in sealed ampoules or flowing								
Ag	5% H_2	0.820	142	−0.646	0.174	0.009	0.688	Through [38]
GaSb	H_2	0.450	131	−0.295	0.155	0.013	0.336	[44]
Ge	Ar, 2% H_2	0.590	155	−0.535	0.055	0.001	0.437	[23]
Hg	100% RH[a]	0.430	130	−0.276	0.154	0.014	0.317	[42]
InSb	Ar	0.390	158	−0.362	0.028	0.001	0.233	Present work
InSb	He	0.480	143	−0.383	0.097	0.005	0.349	Present work
Pb	He	0.406	120	−0.203	0.203	0.025	0.306	[38]
	Averages:	0.509	140	−0.386	0.124	0.010	0.381	
Reactive melts (high dissolved O from substrate [11,38]								
Al	Vacuum	0.844	90	0.000	0.844	0.211	0.772	Through [38]
Co	Ar	1.857	121	−0.956	0.901	0.109	1.752	Through [38]
Fe	H_2	1.673	117	−0.760	0.913	0.125	1.572	Through [38]
Ni	Ar	1.883	120	−0.942	0.942	0.118	1.779	Through [38]
Si	Ar or He	0.826	87	0.043	0.869	0.229	0.757	[38]
	Averages:	1.420	107	−0.523	0.894	0.158	1.326	

[a] 100% relative humidity of water vapor in air at ~20 °C.

4.3. Influence of oxygen

The values of A_{O_2} and B_{O_2} in Table 1 indicate that O_2 increased σ and decreased θ, although the certainty of this conclusion could be higher (i.e., smaller p values), particularly for σ. Thermodynamics provides a good starting point for understanding the interaction between oxygen and molten InSb. First, we consider un-doped InSb in the absence of hydrogen. The standard free energies of formation $\Delta_f G^\circ$ for the oxides at 600 °C are given in the literature as −37 kJ/mol for In_2O_3 [51,74] and ~−475 kJ/mol for Sb_2O_3 [52–54] with oxygen at 1 atm and pure In or Sb. We can calculate the equilibrium oxygen partial pressure P_{O_2} over In_2O_3 in contact with molten InSb. The chemical reaction is

$$2\,\mathrm{In} + 3/2\mathrm{O}_2 = \mathrm{In}_2\mathrm{O}_3 \tag{11}$$

for which the Gibbs free energy change is

$$\Delta G = \Delta_f G^o + RT\ \ln \frac{1}{a_{In}^2 f_{O_2}^{3/2}}, \tag{12}$$

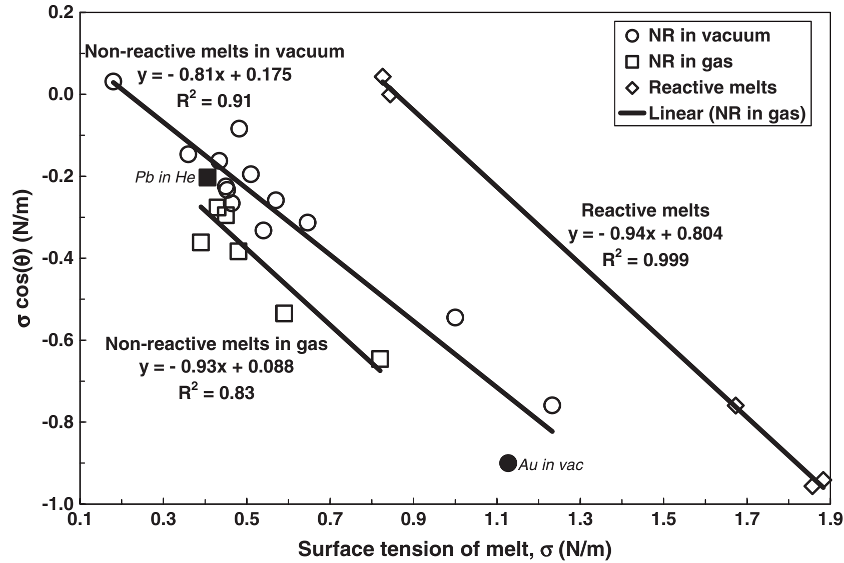

Fig. 11. Literature data for sessile-drop results on liquid metals and semiconductors (see Table 2).

where a_{In} is the activity of In in the liquid and f_{O_2} is the fugacity of O_2 in the gas above solid In_2O_3. At equilibrium $\Delta G = 0$. For an ideal gas and ideal solution (In in InSb), we have $f_{O_2} = P_{O_2}$ and $a_{In} = X_{In} = 0.5$, where X_{In} is the atom fraction of In in the melt. Making these substitutions and solving we find

$$P_{O_2} = a_{In}^{-4/3} \exp\left(\frac{2}{3}\frac{\Delta_f G^\circ}{RT}\right) \text{atm} \, \frac{1.01325 \text{ bar}}{\text{atm}} \approx 10^{-25} \text{ bar}. \tag{13}$$

Similarly, one finds the equilibrium partial pressure of oxygen over Sb_2O_3 to be approximately 10^{-19} bar. Since our experimental P_{O_2} was approximately 10^{-7} bar, this implies that oxide should have covered our drops with no hope of removal (at least in the absence of hydrogen). And yet it did not—shiny oxide-free drops could be obtained in Ar and maintained in Ar and He, provided that O_2 was below about 0.8 ppm. Volatile In_2O must have formed and evaporated. At equilibrium at 600 °C, the partial pressure of In_2O gas over pure In + In_2O_3 is 0.0026 bar, that of In vapor is 1.1×10^{-9} bar, and O_2 is 4×10^{-26} bar [51]. Thus, in our experiments with UHP Ar without H_2, the oxide initially present must have reacted with In to produce In_2O that evaporated until the oxide was gone. Furthermore, In_2O vapor must have continued to form during an experiment.[11] That is, while we did eventually reach a steady state, we never reached equilibrium. This probably explains why σ and θ varied widely, not only from experiment to experiment, but also during a given experiment. The composition of the surface of the drop must have varied, both temporally and spatially, causing σ to vary and probably even causing some Marangoni convection in the drop.

[11] Probably condensing to form the white scaly deposit observed near the exit of the ampoule. Unfortunately, this deposit was not analyzed.

It is interesting that Harter et al. [10] performed their experiments on InSb sealed in an ampoule with an initial $P_{O_2} < 5 \times 10^{-10}$ bar, but with a pressure of approximately 10^{-5} bar upon opening the ampoule. They obtained $\sigma = 0.43$ N/m, which is near our result, but a much lower θ. (Lazrev et al. [55,56] reported $\sigma = 0.42$ N/m). It is interesting that $P_{O_2} = 5 \times 10^{-10}$ bar is still much too large to avoid oxidation of InSb, as found above. It is probable that the H_2 outgassed from the ampoule is sufficient to avoid oxide provided not too much is on the feed material (see Section 4.6).

Another aspect of interest is the amount of O_2 that dissolved in the molten InSb. When O_2 dissolves in liquid metals, it dissociates into single atoms or ions. Thus, we find that the atom fraction X_O is related to P_{O_2} by [57–59]

$$X_O = \frac{\sqrt{P_{O_2}}}{\gamma_O}, \tag{14}$$

where γ_O is the activity coefficient of oxygen atoms/ions in the liquid. For InSb at 600 °C, $\gamma_O = 4.6 \times 10^{-8}$ [59]. The maximum P_{O_2} is that above In_2O_3 in equilibrium with InSb, or from Eq. (13) approximately 10^{-25} bar. Substitution of these values into Eq. (14) gives us $X_O < 6.8 \times 10^{-6} = 6.8$ ppm in order for In_2O_3 not to form. The solubility at 900 °C was estimated to be $X_O = 5.4 \times 10^{-5}$ [59], indicating that the solubility of O increases with increasing temperature. Similarly, dissolution of Sb_2O_3 in Sb at 600 °C gives $X_O = 2.8 \times 10^{-5}$, which increases with increasing temperature [54]. Even though γ_O increases with increasing temperature [59], P_{O_2} above In_2O_3 increases even more [51]. (The solubility of O_2 in liquid metals usually increases with increasing temperature, i.e., the dissolution is usually endothermic (e.g., Ref. [57]).

Changing the temperature of the cell caused momentary changes in the oxygen concentration in the outlet gas. When the temperature was increased, P_{O_2} decreased, and

vice versa. The most likely explanation is that the melt absorbed (dissolved) O_2 when the temperature was increased and vice versa, due to the solubility of O_2 in InSb increasing with temperature. To see if this is reasonable, let us assume a flow rate of 1.6 scfh (0.045 m^3/h) and a decrease in oxygen concentration of 0.035 ppm for 1 s after increasing the temperature from 825 to 873 K. The ideal gas law then gives the amount of oxygen absorbed from the gas into the drop as

$$\left(\frac{1.6\,\text{ft}^3\,\text{gas}}{h}\right)\left(\frac{h}{3600\,\text{s}}\right)(1\,\text{s})\left(\frac{0.035\times10^{-6}\,\text{mol O}_2}{\text{molgas}}\right) \times\left(\frac{\text{mol gas}\cdot K}{0.00290\,\text{atm ft}^3\,\text{gas}}\right)\left(\frac{1\,\text{atm}}{873\,\text{K}}\right) = 7.4\times10^{-12}\,\text{mol O}_2.$$

For a drop weighing 0.4 g and a molecular weight of 236.57, this gives $X_O = 4.4 \times 10^{-9}$, which is only about 0.1% of the maximum O solubility calculated above.

Even for drops that remained shiny and mobile during an experiment, islands of oxide (Fig. 9) formed dull sections when the drops were frozen, while the extruded protrusions remained oxide free. The likely explanation is that rapidly decreasing the drop's temperature reduced the solubility of O so fast that the excess O could not diffuse into the gas stream rapidly enough, and instead formed In_2O_3.

4.4. Influence of inert gas versus vacuum

From Table 2 it is seen that when measurements were made in a vacuum significantly lower values were obtained for θ and σ_{sv}, higher values for W, and little difference in σ. It is particularly meaningful to compare the results for the same substances, InSb and Ge, obtained at high temperature in these two environments. Following are some possible explanations:

- Inert gases tend to have higher partial pressures of O_2 and H_2O than in a good vacuum. As shown in the preceding section, this probably leads to production of In_2O gas at the surface of InSb that prevents formation of solid In_2O_3 and lowers X_O inside the melt. One would expect similar behavior on Ge, with formation of GeO, which sublimes below the melting point of Ge. Because diffusion coefficients in a gas are proportional to $1/P$, the resulting In_2O or GeO would escape much easier in the presence of a vacuum, and lead to a lower X_O in the melt than with an inert gas present. However, as noted earlier O_2 lowers θ for liquid metals on oxide substrates, so that a lower θ would be expected with an inert gas. This is contrary to published results, and so does not provide a likely explanation.
- Since the surface energy σ_{sv} depends on the atomic arrangement at the surface, perhaps the atomic arrangement and bonding of Si and O, both internally and on the surface, depend on the atmosphere in which silica is held. While this at first may seem unlikely, no one appears to have made measurements or done theoretical modeling that would test this idea, particularly at high temperature. Following are two observations that might support such a notion:
  - A fresh surface formed by fracture differs from that formed by fusion (e.g., Ref. [60]). The surface relaxes with time to produce lower energy configurations [61].
  - Fused silica contains a lot of hydrogen, both as dissolved H_2 and chemically bound as SiOH and SiH [62]. "The inherent hydroxyl content of commercial vitreous silica can vary between ~1 ppm and 0.4 mol%" [62]. As noted earlier, this hydrogen diffuses out at in a vacuum at high temperature [2].
- Another potential explanation is the influence of water vapor on the surface of SiO. There are data showing that adsorbed water raises θ on silica for a variety of substances at room temperature, e.g. H_2O (e.g., Refs. [47,63]), organic compounds [47,64] and Hg [31], primarily by lowering σ_{sv}. It is well known that a virgin surface of SiO exposed to air immediately begins to adsorb H_2O and organics. The first H_2O molecules form silanol (≡Si–OH) groups on the surface, until virtually every exposed Si has thus reacted. The amount of silanol is usually characterized by the silanol number α, which is the number of OH/nm of surface [65,66]. Saturation (full hydroxylation) is equivalent to $\alpha_{OH} \approx 4.6\,\text{nm}^{-2}$. Subsequent H_2O is physically adsorbed by hydrogen bonding. The physisorbed H_2O is fully removed in a vacuum at room temperature, or at about 150 °C in air [66]. The chemisorbed H_2O only gradually comes off, for colloidal silica reaching an equilibrium value in vacuum of $a_{OH} \approx 1.5\,\text{nm}^{-2}$ at 600 °C and $0.15\,\text{nm}^{-2}$ at 1100 °C [66]. Fused silica dehydroxylates more readily, reaching $\alpha_{OH} \approx 0.15\,\text{nm}^{-2}$ at 500 °C in vacuum [67]. In dehydroxylation, bridging siloxane groups, ≡Si–O–Si≡, replace silanol groups. The rate of desorption in an inert gas is less than in a vacuum (e.g., Ref. [63]). Furthermore, in a high vacuum the water vapor pressure should be much lower than in an inert gas, so that the equilibrium value of α would be lower. Upon cooling in the presence of water vapor, the surface slowly rehydroxylates [68]. Some siloxane configurations appear much more stable than others [67], so that full rehydroxylation may literally take years of immersion in liquid water at room temperature [66,69] The surface relaxation of silica was shown to be faster in the presence of H_2O [61].

4.5. Influence of choice of inert gas

There are also several possible reasons why θ of InSb was much larger and σ lower in Ar than in He:

- A slight difference in adsorbed water, which is known to increase contact angle (see above). UHP Ar contains

more water than research-grade He. However, we did not measure water content because we believed that adsorbed water would be present at such a low level at 600 °C that it would not matter. Furthermore, we found no difference between results in Ar with preheating at 1100 and at 750 °C.

- The solubility of He in SiO_2 at room temperature is $\sim 20\times$ greater than that of Ar [70]. Dissolved inert gas would be expected to increase the interatomic spacing and thereby increase σ_{sv}, making σ_{sv} larger in He than in Ar, as observed.
- Diffusion coefficients are much higher in He than in Ar. Thus, the transport of O_2 to the melt surface and transport of In_2O away would take place at a higher rate in He. This higher transport would change the O concentration in the melt and on its surface, thereby changing both θ and σ.

4.6. Influence of hydrogen

Addition of hydrogen did not measurably reduce the oxygen concentration in the exiting gas, indicating that negligible reaction between hydrogen and oxygen occurred.[12] The value of $\Delta_f G^\circ$ for H_2O at 600 °C is −200 kJ/mol [71]. From this we can calculate the equilibrium P_{O_2} for 1 ppm of H_2O, 1 ppm of O_2, and 10% H_2 in the feed gas as

$$P_{O_2} = \left(\frac{Y_{H_2O}}{Y_{H_2}}\right)^2 \exp\left(\frac{2\Delta_f G^\circ}{RT}\right) = \left(\frac{3\times10^{-6}}{0.1}\right)^2 \exp\left(\frac{2\times(-2\times10^5)}{8.314\times873}\right) = 1.1\times10^{-33}\ \text{bar}.$$

Thus, the residence time for the gas in the cell of ~2.4 s would have been too short for appreciable reaction at 600 °C.

On the other hand, addition of 10% H_2 to Ar reduced problems with oxide formation on the drops. It is common to add hydrogen to the backfill gas in crystal growth, and experience shows that this greatly diminishes problems with oxide. Our results indicate that hydrogen directly reduced the oxide on our material, probably through the reaction

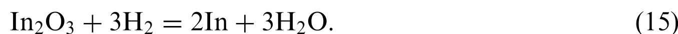

$$In_2O_3 + 3H_2 = 2In + 3H_2O. \quad (15)$$

For $a_{In} = 0.5$, $Y_{H_2O} = 1\times10^{-6}$ and $Y_{H_2} = 0.1$, we calculate the free energy change for this reaction as

$$\Delta G = 3\Delta_f G^\circ_{H_2O} - G^\circ_{In_2O_3} + RT\ \ln\left(\frac{Y^3_{H_2O} a^2_{In}}{Y^3_{H_2}}\right) = -223\ \text{kJ/mol},$$

which reveals a very strong thermodynamic driving force for reaction.

Nevertheless, addition of 10% H_2 to Ar had no measurable influence on θ or σ, probably because once cleaned of oxide there was no change in P_{O_2} at the surface of the drop or of X_O inside the drop.

4.7. Influence of gallium doping

As shown in Figs. 8 and 9, when oxide formed on Ga-doped InSb, Ga was strongly concentrated in the oxide. This is not surprising because $\Delta_f G^\circ$ for Ga_2O_3 at 600 °C is −800 kJ/mol [72,73], which is much more negative than for In_2O_3 and Sb_2O_3 [74–76]. This phenomenon became more pronounced as the oxygen concentration in the gas was increased. One would also expect that oxidation problems would become more severe as the Ga content of InSb is increased.

We found no influence of 0.1% Ga on σ or θ of clean shiny drops.

5. Conclusions

The present work led to the following conclusions:

- The surface tension σ of oxide-free molten InSb was smaller in flowing Ar than in He, probably increased with increasing O_2 in the gas, and was not influenced by 10% H_2 or 0.1% Ga in the melt.
- The contact angle θ on silica was higher in flowing Ar than in He, was lowered by O_2, and was not influenced by H_2 or Ga.
- The work of adhesion W and the surface energy σ_{sv} of the silica were higher in He than in Ar.
- Thermodynamics indicates that oxygen reacted at the surface of the melt to form oxide. When the surface remained oxide free, for <1 ppm O_2 here, In_2O gas must have formed. When solid oxide did form on Ga-doped InSb, it was strongly enriched in Ga, with the Ga/In ratio increasing with the amount of oxygen in the gas.
- The literature shows that the solubility of oxygen atoms or ions in molten InSb decreases with decreasing temperature. A slow temperature decrease caused the excess oxygen to escape into the gas. A rapid temperature decrease during freezing of the drop caused oxide islands to form on the frozen drops surface, giving it a dull appearance. Solid formed from melt extruded from the interior of the freezing drop was shiny and oxide free.
- Examination of published values for liquid metals and semiconductors on silica showed that W and σ_{sv} were highest for reactive melts (in which SiO_2 dissolves). For non-reactive melts, W and σ_{sv} were lower and θ higher in a gas than in a vacuum, regardless of whether the sessile-drop experiments were carried out in sealed ampoules, a flowing gas, or a dynamic vacuum. Thus it appears that the surface of the silica is different in a vacuum that

[12] At equilibrium this reaction would be essentially complete. For example, with 10% H_2 and 100 ppm O_2 supplied with Ar at 1 atm and 600 °C the calculated equilibrium mole fraction of O_2 is approximately 10^{-29}.

at ~1 bar. The reason for this surprising conclusion is unknown.

- Crystal growth is usually carried out in a sealed ampoule. To obtain an oxide-free melt with reduced adhesion (lower *W*) to the ampoule wall it appears advantageous to seal in Ar containing H_2, with carbon also in the ampoule as an added reducing agent. It is surely not a coincidence that this is long-standing common practice with semiconductor crystal growth.

Acknowledgments

This research was supported by NASA Grant NAG 8-1482. We are grateful to William Micklethwaite of Firebird Semiconductors for furnishing the InSb and for his advice, interest and encouragement. We greatly appreciate stimulating discussions and email exchanges with Thierry Duffar and with Frank Szofran and co-workers.

References

[1] W. Palosz, J. Crystal Growth 267 (2004) 475.
[2] W. Palosz, J. Crystal Growth 267 (2004) 484.
[3] W. Palosz, J. Crystal Growth 191 (1998) 897.
[4] L.L. Regel, W.R. Wilcox, Microgravity Sci. Technol. 14 (1999) 152.
[5] J. Wang, L.L. Regel, W.R. Wilcox, J. Crystal Growth 260 (2004) 590.
[6] M.P. Volz, M. Schweizer, N. Kaiser, S.D. Cobb, L. Vujisic, S. Motakef, F.R. Szofran, J. Crystal Growth 237–239 (2002) 1844.
[7] S.D. Cobb, F.R. Szofran, K.S. Jones, S.L. Lehoczky, J. Electron. Mater. 28 (1999) 732.
[8] Y. Wang, L.L. Regel, W.R. Wilcox, J. Crystal Growth 143 (2002) 546.
[9] T. Duffar, P. Boiton, P. Dusserre, J. Abadie, J. Crystal Growth 179 (1997) 397.
[10] I. Harter, P. Dusserre, T. Duffar, J.Ph. Nabot, N. Eustathopoulos, J. Crystal Growth 131 (1993) 157.
[11] N. Eustathopoulos, M.G. Nicholas, B. Drevet, Wettability at High Temperatures, Pergamon/Elsevier, Oxford, 1999, pp. 218–239.
[12] Ju.V. Naidich, in: D.A. Cadenhead, J.F. Danielli (Eds.), Progress in Surface and Membrane Science, vol. 14, Academic Press, New York, 1981, p. 354.
[13] H. Taimatsu, T. Tani, H. Kaneko, J. Mater. Sci. 31 (1996) 6383.
[14] A. Sharan, A.W. Cramb, Met. Mater. Trans. B 28B (1997) 465.
[15] N. Eustathopoulos, B. Drevet, M.L. Muolo, Mater. Sci. Eng. A 300 (2001) 34.
[16] H. Taimatsu, M. Abe, F. Nakatani, K. Ogino, Nippon Kinzoku Gakkaishi/J. Jpn. Inst. Met. 49 (1985) 523.
[17] X. Huang, S. Togawa, S. Chung, K. Terashima, S. Kimura, J. Crystal Growth 156 (1995) 52.
[18] Z. Niu, K. Mukai, Y. Thiaishi, T. Hibiya, K. Kakimoto, M. Koyama, J. Jpn. Assoc. Crystal Growth 24 (1997) 31.
[19] Z. Niu, K. Mukai, Y. Shiraishi, T. Hibiya, K. Kakimoto, M. Koyama, in: N. Eustathopoulos, N. Soczak (Eds.), Proceedings of the International Conference on High Temperature Capillarity, Cracow, Poland, 1997, pp. 175–181.
[20] Z. Niu, K. Mukai, Y. Shiraishi, T. Hibiya, K. Kakimoto, M. Koyama, in: V.S. Avduyevsky, V.I. Polezhaev (Eds.), Proceedings of the Joint Xth European and VIth Russian Symposium on Physical Sciences in Microgravity, vol. II, Moscow, 1997, pp. 48–55.
[21] M. Ratto, E. Ricci, E. Arato, J. Crystal Growth 217 (2000) 233.
[22] K. Mukai, Z. Yuan, K. Nogi, T. Hibiya, ISIJ Int. 40 (Suppl.) (2000) S148.
[23] N. Kaiser, A. Cröll, F.R. Szofran, S.D. Cobb, K.W. Benz, J. Crystal Growth 231 (2001) 448.
[24] A.K. Kota, M.S. Thesis, Clarkson University, Potsdam, NY, 2003.
[25] S. Ramakrishnan, M.S. Thesis, Clarkson University, Potsdam, NY, 2003.
[26] G. Anand, M.S. Thesis, Clarkson University, Potsdam, NY, 2005.
[27] A.C. Bovik, Handbook of Image and Video Processing, Academic Press, San Diego, CA, 2000.
[28] A.W. Neumann, R.J. Good, in: R.J. Good, R.R. Stromberg (Eds.), Surface and Colloid Science, vol. 11, Plenum Press, New York, 1979, p. 31.
[29] S. Lahooti, O.I. Del Rio, A.W. Neumann, P. Cheng, in: A.W. Neumann (Ed.), Applied Surface Thermodynamics, Marcel Dekker Inc., New York, 1996.
[30] F. Bashforth, J.C. Adams, An Attempt to Test the Theory of Capillary Action, Cambridge University Press, Cambridge, England, 1892.
[31] A. Carré, N. Visovsky, J. Adhes. 68 (1998) 301.
[32] A. Carré, M.E.R. Shanahan, J. Adhes. 49 (1995) 177.
[33] I. Harter, P. Dusserre, T. Duffar, J.-Ph. Nabot, N. Eustathopoulos, J. Crystal Growth 131 (1993) 157.
[34] A.W. Adamson, Physical Chemistry of Surfaces, second ed., Interscience/Wiley, New York, 1967.
[35] P. Roura, J. Fort, J. Colloid Interface Sci. 272 (2004) 420.
[36] D.Y. Kwok, C.N.C. Lam, A. Li, A. Leung, R. Wu, E. Mok, A.W. Neumann, Colloids Surf. A: Physicochem. Eng. Aspects 142 (1998) 219.
[37] D.Y. Kwok, A.W. Neumann, Adv. Colloid Interface Sci. 81 (1999) 167.
[38] R. Sangiorgi, M.L. Muolo, D. Chatain, N. Eustathopoulos, J. Am. Ceram. Soc. 71 (1988) 742.
[39] R. Shetty, R. Balasubramanian, W.R. Wilcox, J. Crystal Growth 100 (1990) 51.
[40] H. Chiriac, M. Tomut, C. Naum, F. Necula, V. Nagacevschi, Mater. Sci. Eng. A 226–228 (1997) 341.
[41] R. Shetty, R. Balasubramanian, W.R. Wilcox, J. Crystal Growth 100 (1990) 58.
[42] R.J. Good, J.K. Paschek, in: J.F. Padday (Ed.), Wetting, Spreading and Adhesion, Academic Press, New York, 1978, pp. 147–160.
[43] A. Amirfazli, D. Chatain, A.W. Neumann, Colloids Surf. A: Physicochem. Eng. Aspects 142 (1998) 183.
[44] A. Cröll, R. Lantzsch, S. Kitanov, N. Salk, F.R. Szofran, A. Tegetmeier, Crystal Res. Technol. 38 (2003) 669.
[45] R.J. Good, in: R.J. Good, R.R. Stromberg (Eds.), Surface and Colloid Science, Vol. I: Experimental Methods, Plenum Press, New York, 1979, p. 7.
[46] J.K. Spelt, D. Li, in: A.W. Neumann, J.K. Spelt (Eds.), Applied Surface Thermodynamics, Marcel Dekker, New York, 1996, pp. 239–292 (through [37]).
[47] B. Janczuk, A. Zdziennicka, J. Mater. Sci. 29 (1994) 3559.
[48] O.V. Mazurin, M.V. Streltsina, T.P. Shvaiko-Shvaikovskaya, Handbook of Glass Data, Part A: Silica Glass and Binary Silicate Glasses, Elsevier, Amsterdam, 1983 (through V).
[49] A. Roder, W. Kob, K. Binder, J. Chem. Phys. 114 (2001) 7602.
[50] Yu.K. Shchipalov, Glass Ceram. 57 (2000) 374.
[51] D. Chatterji, R.W. Vest, J. Am. Ceram. Soc. 55 (1972) 575.
[52] D. Chatterji, J.V. Smith, J. Electrochem. Soc. 120 (1973) 889.
[53] P. Knauth, G. Schwitzgebel, Ber. Bunsenges. Phys. Chem. 92 (1988) 32.
[54] K.T. Jacob, P.M. Mathew, Z. Metallkunde 70 (1979) 366.
[55] V.B. Lazrev, Russ. J. Phys. Chem. 38 (1964) 172 (through [9]).
[56] M.Y. Dashevski, G.V. Kukuladze, V.B. Lazrev, M.S. Mirgalovskii, Izv. Akad. Nauk SSSR, Neorg. Mater. 3 (1967) 1561 (through [9]).
[57] O. Kubaschewski, A. Cibula, D.C. Moore, Gases and Metals, American Elsevier Publishing Co., New York, 1970, pp. 11–18.
[58] A. Sieverts, Z. Metallkunde 21 (1929) 37.
[59] T.L. Ngai, R. Schmid-Fetzer, Z. Metallkunde 82 (1991) 289.
[60] E.A. Leed, C.G. Pantano, J. Non-Cryst. Solids 325 (2003) 48.

[61] A. Agarwal, M. Tomozawa, J. Non-Cryst. Solids 209 (1997) 264.
[62] J.E. Shelby, J. Appl. Phys. 48 (1977) 3387.
[63] A. Kanta, R. Sedev, J. Ralson, Langmuir 21 (2005) 2400.
[64] M.K. Bernett, W.A. Zisman, J. Colloid Interface Sci. 29 (1969) 413.
[65] E.R. Vansant, P. VanDerVoort, K.C. Vrancken, Characterization and Chemical Modification of the Silica Surface, Elsevier, Amsterdam, 1995.
[66] L.T. Zhuravlev, Colloids Surfaces A: Physicochem. Eng. Aspects 173 (2000) 1.
[67] A.S. D'Souza, C.G. Pantano, J. Am. Ceram. Soc. 85 (2002) 1499.
[68] B.J. Wood, R.N. Lamb, C.L. Rason, Surf. Interface Anal. 23 (1995) 680.
[69] M.H. Du, A. Kolchin, H.P. Cheng, J. Chem. Phys. 120 (2004) 1044.
[70] J.S. Flores, J.F. Shackelford, J. Non-Cryst. Solids 68 (1984) 327.
[71] JANAF Thermochemical Tables, third ed., American Chemical Society; J. Phys. Chem. Ref. Data 14 (Suppl. 1) (1985) 1272.
[72] J.V. Smith, D. Chatterji, J. Am. Ceram. Soc. 56 (1973) 288.
[73] M. Zinkevich, F. Aldinger, J. Am. Ceram. Soc. 87 (2004) 683.
[74] L.B. Pankratz, Thermodynamic Properties of Elements and Oxides, US Government Printing Office, Washington, DC, 1982.
[75] S.C. Schaefer, The Free Energy of Formation of Indium Oxide by EMF Measurements, no. 7549, US Bureau of Mines, Department of the Interior, 1971.
[76] R.C. Weast, M.J. Astle, W.H. Beyer, CRC Handbook of Chemistry and Physics, 66th ed., CRC Press, Boca Raton, FL, 1985, p. F-164.